ELSEVIER

Journal of Structural Geology 28 (2006) 456–473

JOURNAL OF STRUCTURAL GEOLOGY

www.elsevier.com/locate/jsg

Late Paleozoic strike-slip faults and related vein arrays of Cape Elizabeth, Maine

Mark T. Swanson

Department of Geosciences, University of Southern Maine, Gorham, ME 04038, USA

Received 25 May 2004; received in revised form 14 March 2005; accepted 2 December 2005
Available online 7 February 2006

Abstract

Strike-slip faults and related quartz vein arrays of Late Paleozoic-age cut gently-dipping metasedimentary rocks at Cape Elizabeth in southern coastal Maine and formed in response to regional dextral shearing along the Norumbega fault system. Vertical quartz veins up to 20 m wide and 10s of meters long were emplaced orthogonal to the local shear zone-parallel elongation fabric, reflecting strain partitioning during transpression. Earlier veins were reoriented by clockwise rotation toward this NE-trending regional shear direction. The later brittle strike-slip faults are oblique to the regional shear direction and interpreted as a 10-km-scale R-shear array on the southeast flank of the Norumbega fault system. These left-stepping en échelon fault zones consist of the three Two Lights fault zones (~200 m lengths and up to ~5 m displacements) and the Richmond Island fault zone (~1.6 km length and ~40 m displacement). Displacements on these fault zones have developed fine-grained silicified, obliquely-foliated and laminated cataclasites and locally, millimeter-thin pseudotachylyte fault and injection veins. Individual fault core zones are up to 10s of centimeters thick as part of several complex anastamosing zones of faulting 10s of meters wide. Initial segments within each fault zone are typically terminated with oblique extension fractures in horsetail configurations. The left-stepping en échelon relationships between these segments led to dominantly contractional step-over zones where P-shear linkages created a through-going fault that truncated the ends of the earlier-formed terminated segments. This linkage-growth model for fault zone evolution works toward larger scales and longer fault lengths as displacement accumulates, within a limiting maximum displacement/length ratio characteristic of the host lithologies. Length–frequency data for fault segments within these zones suggest a transition to linkage-dominated growth once fault segments were longer than ~15 m. Continued displacement was accommodated along the P-shear linked en échelon faults through imbrication, contractional duplexing and adhesive wear on the outcrop-scale. Core zone processes on the micro-scale reflect cataclasis and frictional sliding during coseismic slip as well as cataclastic flow and pressure solution during post-seismic creep. The development of foliated-to-laminated cataclasite was accompanied by pore volume collapse, pressure solution and fluid expulsion that, in turn, triggered the development of the late fault-related quartz vein arrays.

Keywords: Strike-slip faults; Quartz veins; Fault growth

1. Introduction

Strike-slip faults are notably segmented at all scales and levels of exposure (Tchalenko, 1970; Segall and Pollard, 1980; Barka and Kadinsky-Cade, 1988; Sylvester, 1988; Scholz, 1990; Vermilye and Scholz, 1999), typically in the form of en échelon shear fractures. The step-over zones of host rock between the ends of en échelon shear fractures deform in order to accommodate continued displacement and eventual linkage to a through-going fault zone (Fig. 1). The geometry of these step-over zones and linking fault structures, in turn, controls the overall style of fault zone development.

The different shear and extension fractures found associated with shallow crustal fault zones (Fig. 1) have been characterized through detailed field studies of exhumed fault structures (Tchalenko, 1970; Grocott, 1981; Hedgecoxe and Johnson, 1986; Swanson, 1988, 1989, 1990, 2005; Cruikshank et al., 1990, 1991; Arboleya and Engelder, 1995; Davis et al., 1999) and a history of experimental modeling (Riedel, 1929; Morgenstern and Tchalenko, 1967; Tchalenko, 1970; Logan et al., 1979; Bartlett et al., 1981; Naylor et al., 1986; Arch et al., 1988). Model studies using materials such as clay and sand (e.g. Riedel, 1929; Wilcox et al., 1973) have revealed a fairly consistent pattern of development in experimental fault zones. Fault zones in clay, for example, usually begin with an early fabric of small R-shears and minor R′-shears that evolves into larger en échelon R-shears. P-shear linkage, imbrication and duplexing (Fig. 1) combine to give a through-going but irregular fault zone as seen in natural examples

E-mail address: mswanson@usm.maine.edu

0191-8141/$ - see front matter © 2006 Elsevier Ltd. All rights reserved.
doi:10.1016/j.jsg.2005.12.009

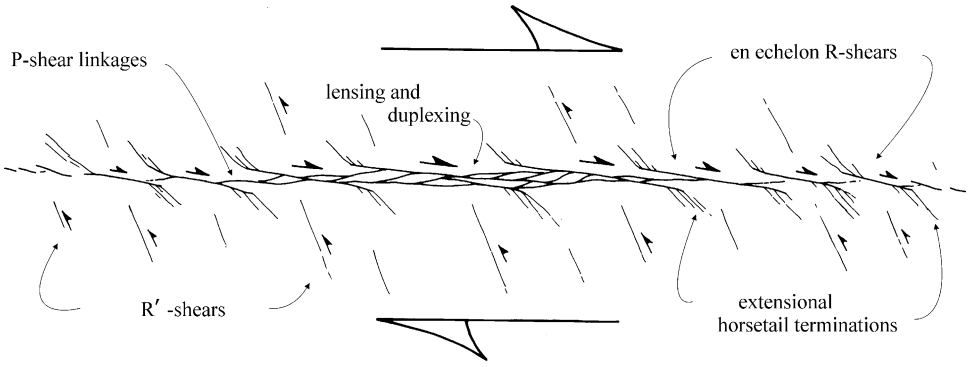

Fig. 1. Fault zone terminology includes en échelon R-shears, R′-shears and oblique extension-fracture terminations. Initial en échelon R-shear arrays develop P-shear linkages, lenses and duplexes to form through-going fault zones.

and experimental studies (Riedel, 1929; Tchalenko, 1970; Tchalenko and Ambraseys, 1970; Bartlett et al., 1981; Naylor et al., 1986; Woodcock and Fischer, 1986; Arch et al., 1988; Cruikshank et al., 1991).

Faulting in the upper crust has also been characterized (Sibson, 1989, 1990; Hickman et al., 1995; Janssen et al., 1997) as a seismo-structural process that involves stress cycling, coseismic displacements, post-seismic creep and the formation and collapse of fault-related dilatancy driving transient pulses of hydrothermal fluids. Fault 'valve' models have been proposed (Cox, 1995; Robert et al., 1995; Nguyen et al., 1998) where increasing fluid pressures below sealed reverse faults periodically trigger displacements with subsequent enhanced fluid flow and re-silicification. Fault 'pump' models have also been proposed (Sibson et al., 1975), where coseismic collapse of strain-induced micro-crack dilatancy within the host rock flushes fluid through the broken fault zone rock (Matthai and Fisher, 1996). Post-seismic creep and compaction of newly formed cataclasite (Sleep and Blanpied, 1994; Segall and Rice, 1995), in turn, lead to pore volume reduction with fluid expulsion and vein emplacement in the adjacent wall rocks (Renard et al., 2000).

The Cape Elizabeth fault zones studied here (Fig. 2) are associated with pseudotachylyte as evidence of frictional melting and coseismic slip as well as abundant quartz veins as evidence of transient fluid flow, both characteristics of earthquake faulting (Scholz, 1988, 1990; Sibson, 1989). The mapping of these exhumed structures provides a detailed view of these strike-slip fault/vein systems adding to our understanding of the processes of fault zone evolution and the deformation mechanisms involved in earthquake generation.

2. Geology of the Cape Elizabeth study area

The strike-slip fault zones and related veins described in this paper are exposed in coastal terraces in the vicinity of Two Lights State Park and adjacent Richmond Island in Cape Elizabeth, Maine (Fig. 2), at the southern end of Casco Bay.

2.1. Structural setting

The host rocks at these localities consist of chloritized garnet-bearing phyllitic quartzites that are correlated with the Lower Paleozoic Kittery Formation of the Merrimack Group of southern Maine and New Hampshire (Hussey, 1988; Bothner and Hussey, 1999). The exposures at Cape Elizabeth are separated from the rest of the highly sheared Casco Bay area by the Broad Cove shear zone, considered to be one of the principal splays (Bothner and Hussey, 1999) of the Late Paleozoic-age Norumbega fault/shear zone system (Fig. 2). The restraining bend geometry in the Casco Bay area (Osberg et al., 1985; Swanson, 1992, 1999a,b) contributed to the formation of regional scale en échelon isoclinal upright F_2 folds, oblique to the main Norumbega fault zone, which

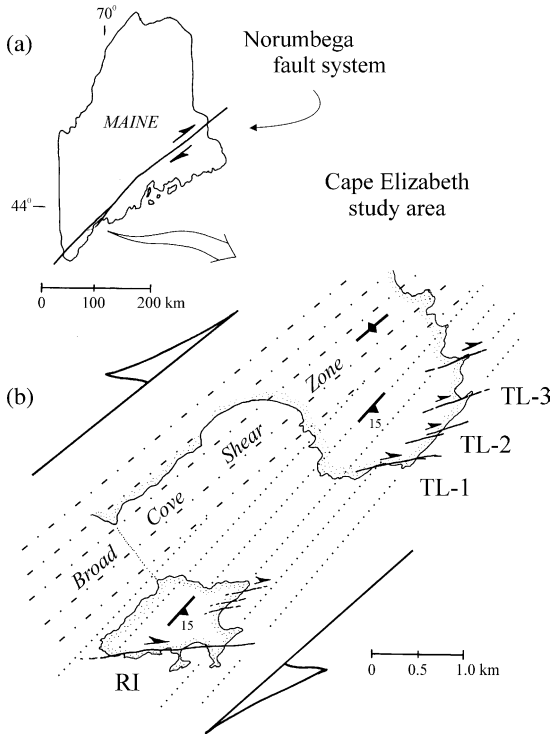

Fig. 2. Location and structural setting for the Cape Elizabeth fault zones. (a) Regional setting of the Norumbega fault system with the location of the study area. (b) Specific fault zones in Cape Elizabeth include the Two Lights fault zones (TL-1, TL-2 and TL-3) and Richmond Island fault zone (RI). Dashed and dotted lines represent the host rock layering within and adjacent to the Broad Cove shear zone, an outer splay to the Norumbega shear zone system. Strike and dip symbols in (b) represent the gently SE-dipping fold limbs in the Two Lights exposures and the vertical flow layering in the Broad Cove shear zone.

became reoriented and sheared into the main fault trace as the transpressional deformation continued.

This regional Norumbega-shearing is expressed in a wide variety of strain and kinematic indicators (Swanson, 1992, 1999a) throughout the oblique F_2 folds on the southeast side of the main fault zone. The steeply-dipping host rock layering within this folded terrain helped to partition the transpression into layer-parallel simple shear as the translation component, and a horizontal layer-parallel elongation (and accompanying layer-normal shortening) as the pure shear component to the deformation. The local crustal thickening associated with this transpression led to uplift, erosional unroofing and cooling of the present-day crust through the brittle–plastic transition where progressive strain hardening promoted the development of the brittle strike-slip faults.

The Two Lights and Richmond Island exposures southeast of the Broad Cove shear zone and outside of the higher shear strain zones in Casco Bay, reveal a gently southeast dipping planar S_0/S_1 anisotropy (related to recumbent F_1 folds) with only open to gentle upright F_2 folds (Fig. 2b). The cataclastic strike-slip faults in these exposures cut obliquely across this gently SE-dipping lithological layering and are distributed along the southeast flank of the much larger NE-trending Broad Cove shear zone.

2.2. Age and depth of exposure for the Cape Elizabeth fault zones

The age of these Late Paleozoic strike-slip faults can be constrained by $^{40}Ar/^{39}Ar$ ages on biotites (West, 1988; West et al., 1989) from the sheared metamorphic rocks on the southeast side of the main Norumbega zone. These biotite ages indicate that the onset of brittle faulting due to post-metamorphic uplift and cooling below the 300 °C closure temperature for biotite would have occurred at ~290–295 my during the latest Carboniferous. Early Permian K/Ar whole rock ages of 270 ± 32 and 277 ± 16 my were also reported by Bothner and Hussey (1999) for pseudotachylyte from related(?) fault structures in the Fort Foster Brittle Zone (Swanson, 1988) of southernmost Maine.

Pressure estimates of 2.3–3.0 kbars for Late Devonian peak metamorphism in the Saco-Harpswell sequence on the southeast side of the main Norumbega zone as reported by Dunn and Lang (1988) represent maximum former crustal depths of ~8–10 km. Later retrograde chloritization commonly associated with the Cape Elizabeth faults and veins as well as the regional Norumbega fault system (Hussey, 1985) also indicates progressively shallower crustal levels likely due to uplift and erosion. Further erosion into the Mesozoic yields crustal depths of 5.3–7.6 km and temperatures of only 170–200 °C (Dougherty and Lyons, 1980) based on zircon-apatite ages for younger Jurassic plutons in nearby New Hampshire.

The pseudotachylyte-bearing strike-slip faults in the Cape Elizabeth area, then, are latest Carboniferous to Permian in age (300–250 my) developed at ~2.0 kbars, ~250–300 °C, and ~7–8 km depth during the waning stages of oblique convergence and associated dextral transpression. These conditions reflect former crustal depths for the exposed fault zones above the brittle–plastic transition (Scholz, 1990), where

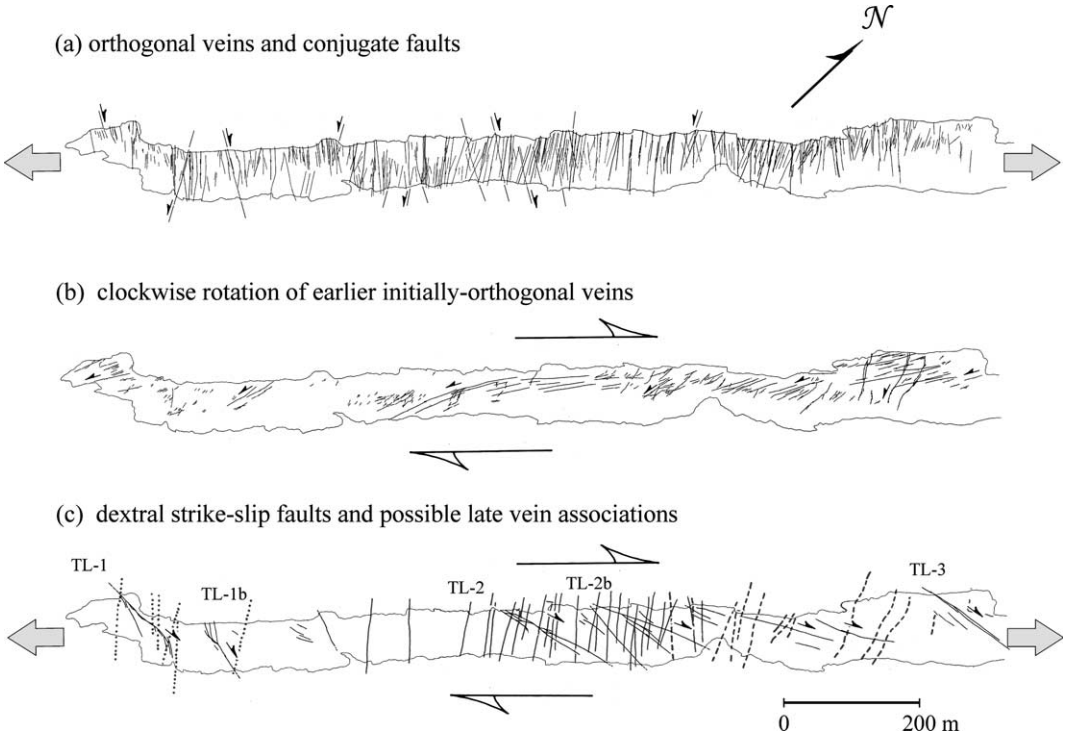

Fig. 3. Two Lights shoreline exposure showing the orientation and distribution of selected structures developed during shearing and extension. (a) Latest undeformed orthogonal vein array and small dihedral angle planar conjugate strike-slip faults with extension due to strain partitioning during transpression. (b) Variably deformed quartz veins reoriented by clockwise rotation and antithetic (sinistral) slip due to dextral shearing. (c) Oblique dextral strike-slip faults including the TL-1, TL-2, and TL-3 fault zones and vein associations with the youngest undeformed to slightly deformed, initially orthogonal-to-shear vein arrays.

deformation is dominated by brittle fracturing at high intermittent strain rates and diffusive mass transfer/solution creep at low background strain rates (Knipe, 1989; Gratier and Gamond, 1990).

3. Quartz vein emplacement and deformation by dextral shear

The gently SE-dipping lithologies in the Cape Elizabeth exposures are just 1 km outside of the main Casco Bay shear zones but have still developed a distinctive NE-trending sub-horizontal stretching lineation that defines an elongation/shear flow fabric parallel to the regional shear direction (Fig. 2b). NW-trending quartz–ankerite–chlorite-filled veins perpendicular to the lineation in these outcrops (Fig. 3a) are typically only a few centimeters thick and 10s of meters long but can be as much as 20 cm thick. Swanson (1992, 1999a) documented the initial emplacement of quartz veins orthogonal to this elongation/shear flow fabric (as the layer-parallel elongation component of the strain-partitioned transpression) with clockwise reorientation to lower angles (Figs. 3b and 4a and b) caused by continuous dextral shear. These syn-tectonic quartz veins vary in orientation that can be related to age of emplacement. Younger, less deformed veins at higher angles to the shear direction consistently cross-cut the older more deformed veins and boudin strings at lower angles to the shear direction. The clockwise rotation of poles to veins as seen in stereogram (Fig. 4a and b) creates a great circle distribution that defines a steeply-plunging rotation axis for the observed dextral shear. A histogram of vein orientations relative to the shear direction (Fig. 5a) in the Two Lights exposures reveals a continuum of positions suggesting intermittent veining throughout the period of dextral shear (see stereogram Fig. 4b). The apparent triple peak structure in the smoothed histogram (Fig. 5a) may suggest possible long-term fluctuations in fluid pressure during shear or variations in strain rate during veining but it likely represents a bias in the distribution where the intense development of certain vein sets in localized areas dominate the data.

While the strike-slip faults cut the earlier deformed and reoriented veins and boudin strings, cross-cutting relations between the strike-slip faults and the youngest vein sets are contradictory. This suggests a broadly contemporaneous relationship between the brittle strike-slip faulting and the later part of a protracted history of episodic veining and

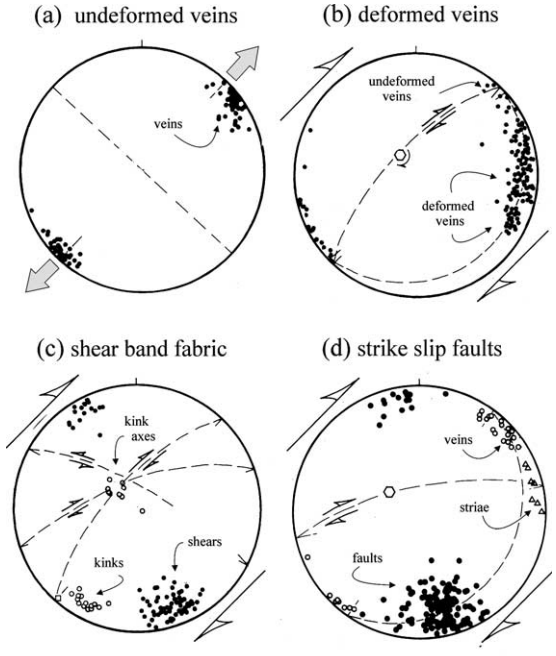

Fig. 4. Structural data in stereograms for the Cape Elizabeth exposures. (a) Poles to latest undeformed quartz veins orthogonal to shear zone-parallel extension. (b) Poles to quartz veins deformed by regional dextral shear with reorientation of initially orthogonal-to-shear undeformed veins by clockwise rotation under a steeply-plunging rotation axis reconstructed from the great circle distribution of poles to reoriented veins. (c) Poles to low angle dextral shear bands and high-angle sinistral kink-bands with steeply-plunging rotation axes that are interpreted as an R–R′ conjugate shear set reflecting dextral strike-slip. (d) Fault striations and poles to dextral faults and termination veins show a sub-horizontal great circle distribution characteristic of strike-slip. Arrows indicate the NE–SW extension and NE-trending dextral strike-slip associated with the transpressional deformation.

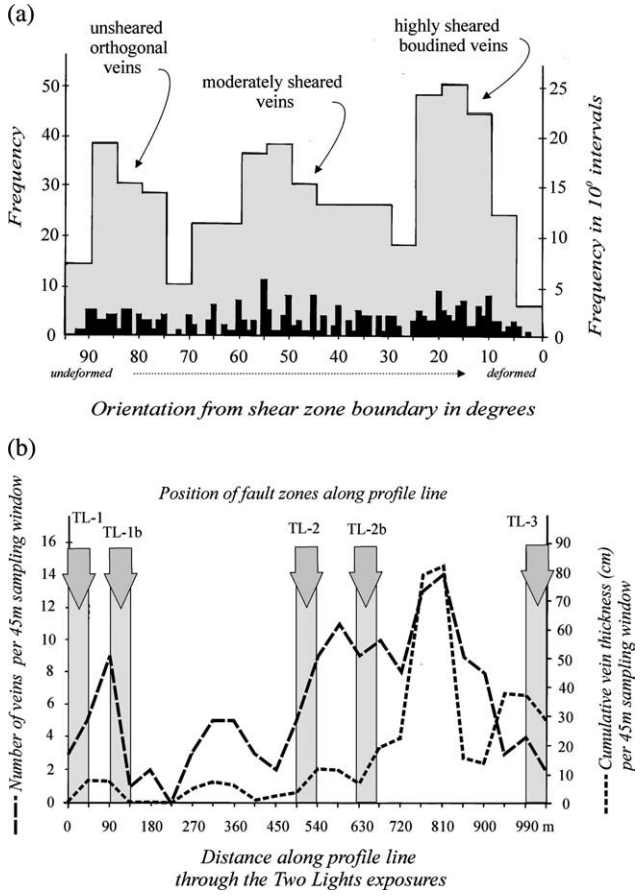

Fig. 5. Quartz vein distribution in the Two Lights shoreline exposures. (a) Histogram of vein orientations relative to the interpreted shear direction showing a continuum of trends with three possible clusters of vein orientations. (b) Profile line along the length of the Two Lights exposures. There is an increase in vein intensity and vein extension associated with each of the TL-fault zones. High values between the TL-2 and TL-3 fault zones are due to multiple faults with overlapping vein arrays.

regional shear. There appear to be specific sets of veins spatially associated with each of the main fault zones (Fig. 3c). A profile line through the mapped Two Lights exposures (Fig. 5b) shows an increase in vein intensity and extension associated with the areas immediately surrounding each of the TL-fault zones. The vein arrays associated with the TL-1 and TL-2 fault zones are similar in mineralogy and orientation but are spatially separated by a gap in vein intensity and extension. At the eastern end of the Two Lights exposure the increase in extension and intensity between the TL-2 and TL-3 fault zones may be attributed to overlapping vein systems due to the proximity of the two faults.

The latest extensional structures are conjugate sets of very planar high-angle-to-shear brittle strike-slip faults that include WNW-trending dextral and NNW-trending sinistral structures (Fig. 3a) that indicate a similar NE–SW extension direction as the orthogonal-to-shear quartz veins. Such late conjugate faults in shear zones have been described by Nguyen et al. (1998) and Poulsen and Robert (1989) and are similar to the X–X′ faults of Logan et al. (1979) and Swanson (1988). The change in deformation response from pure shear extension fracturing to the small dihedral angle, hybrid, extension/shear fracturing could be related to variations in local fluid pressures and differential stress at the time of deformation.

4. The Two Lights and Richmond Island Fault Zones

The exposure at Two Lights State Park (Figs. 2 and 3) is 1.2 km long and 50 m wide, is aligned parallel to the interpreted regional shear direction and contains numerous strike slip fault zones. The three major Two Lights fault zones, (TL-1, TL-2, and TL-3 from west to east) have displacements in the 3–5 m range. The nearby Richmond Island shoreline exposure is ~600 m long aligned parallel to the Richmond Island fault zone (Fig. 2), which has a larger displacement of ~40 m.

The TL and RI fault zones were mapped using a variety of techniques that included the use of measuring tape grids at a scale of 1:60, a 7 m camera pole and aerial photo mosaic, and a plane table and alidade at a scale of 1:120. The maps of the Two Lights and Richmond Island fault zones (Fig. 6) have been reduced in size for publication so that considerable detail and complexity cannot be shown. Detailed views of selected areas are provided in the subsequent figures to show the characteristic structures within each of the mapped faults.

4.1. Bulk dextral shear

A late stage of dextral shear throughout these exposures is reflected in locally prominent centimeter-to-meter long dextral shear bands (Figs. 4c and 7b) that cut obliquely across the elongation/shear flow fabric (Swanson, 1992, 1999a), particularly in the more phyllitic layers. Centimeter-wide sinistral strike-slip kink bands at high angles to the elongation/shear flow fabrics also occur with steeply-plunging rotation axes (72° towards 320°). These sinistral kink bands (Fig. 7b) are interpreted as antithetic R′-shears related to regional dextral shearing. These are in a conjugate relationship to the dextral R-shear bands where the acute bisector between the two sets reflects the paleostress orientation for dextral shearing. The larger 100+-m-long dextral cataclastic fault zones are similar in orientation to the smaller scale shear band fabric elements and are also interpreted as R-shears (Figs. 2 and 3c). This pattern of conjugate strike-slip structures with NNE-trending dextral shear band fabrics and NNW-trending sinistral kink bands is similar to the left lateral strike-slip faults and right-lateral monoclinal kink bands in the Sierra Nevada (Davies and Pollard, 1986), and to the conjugate arrays in proto-Riedel shear zones in Navajo sandstone of southern Utah described by Ahlgren (2001).

4.2. Fault orientations and kinematics

The Two Lights and Richmond Island fault zones have a general 080° strike and 75°NW dip, oblique to the 042° trend of the regional F_2 hinge-parallel lineation that defines the elongation/shear flow fabric and interpreted regional shear direction. Each of these oblique faults is composed of ENE-trending dextral strike-slip fault zones and NW-trending extension veins. The stereogram of fault striations and poles to slip surfaces and veins within these fault zones (Fig. 4d) shows a nearly-horizontal great circle distribution, representing the movement plane during faulting, and a steeply-plunging kinematic rotation axis (66° towards 055°) that approximates the intermediate principal stress direction for plane strain during the deformation. Rare centimeter-wide grooves in cataclastic sheets along some of the main fault surfaces (Fig. 4d) are also gently-plunging (~8° NE) indicating a subhorizontal shear direction. NNW-trending sinistral strike-slip kink-bands are also common within, and adjacent to, the individual dextral fault zones. The oblique orientation of these fault zones relative to the overall shear direction, their dextral shear sense and left-stepping en échelon geometry support their interpretation as outcrop-scale en échelon R-shear fault zones (Figs. 2 and 3c) in a kilometer-wide zone of dextral strike-slip shearing.

4.3. Types of fault-related rocks and structures

The Cape Elizabeth fault zones have produced quartz, ankerite and chlorite veins (Figs. 7a and 8c), quartz- and calcite-cemented dilation breccias (Figs. 7f and 8a), finer-grained cataclasites (Fig. 7c and h), obliquely-foliated cataclasites (Figs. 7g and 8e and f), laminated cataclasites (Fig. 8g and h) and local pseudotachylyte fault and injection veins (Fig. 8b and d). The faults display narrow core zones (Fig. 7c) with laminated ultracataclasite (Fig. 8g and h), and flanking damage zones (Fig. 7e and f) with minor breccias (Figs. 7f and 8a and b), splay faults (Fig. 7d), shear band fabrics (Fig. 7b), kink bands (Fig. 7b) and extension veins (Fig. 7a). Individual cataclastic core zones vary in width depending on the magnitude of displacement but typically range up to ~1–2 cm for the Two Lights faults (Figs. 7c and 8g and h) and up to 10s of centimeters for the Richmond Island fault zone (Fig. 7h).

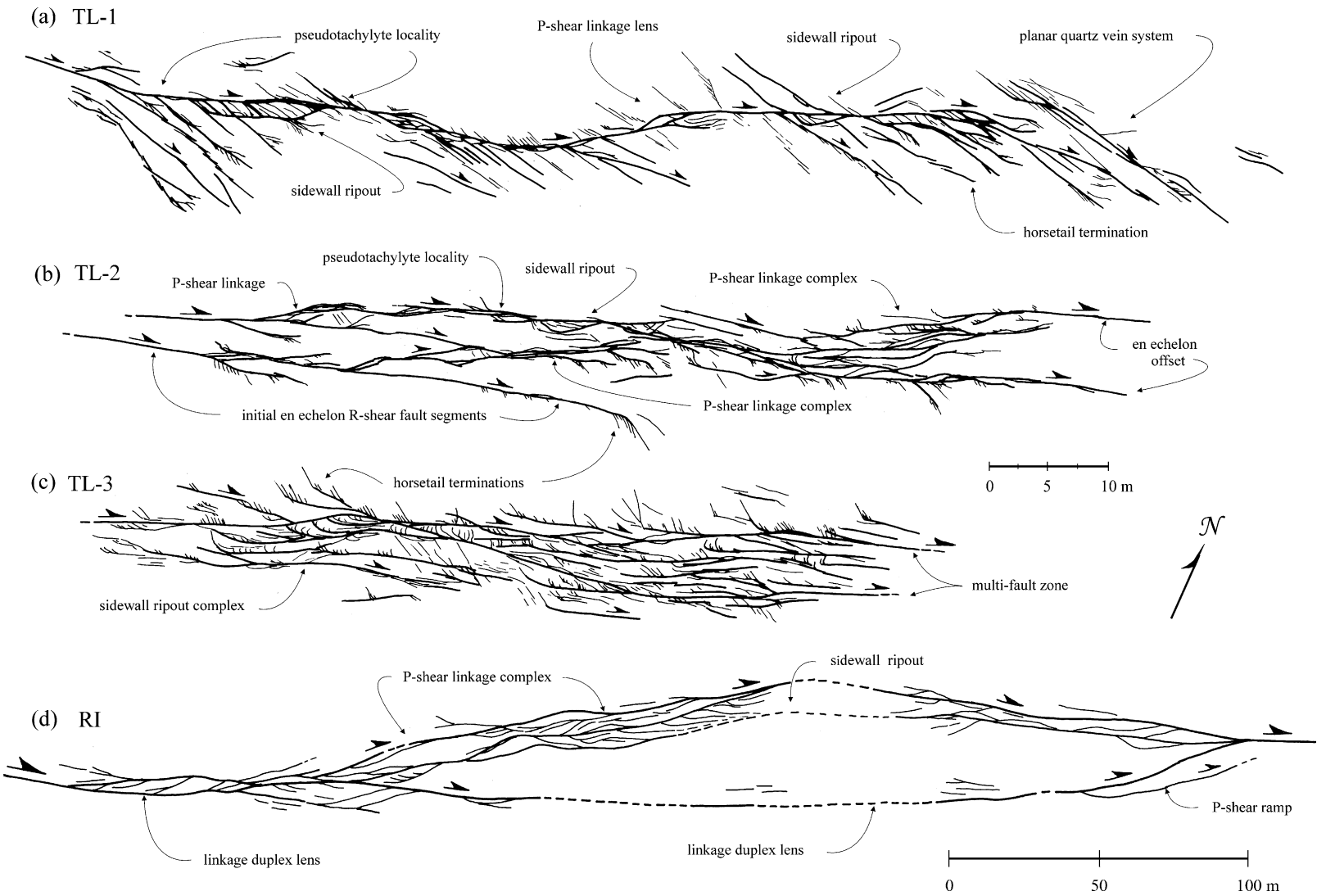

Fig. 6. Maps of the Two Lights and Richmond Island fault zones in the Cape Elizabeth exposures. (a) TL-1 fault as a through-going fault zone with wall rock lensing through a high-angle oblique vein and fracture array. (b) TL-2 fault with low-angle initial en échelon array, discrete linkage structures and final through-going fault zone. (c) TL-3 fault zone with a broad zone of multiple sub-parallel fault surfaces, abundant extension fractures and termination arrays. (d) RI fault zone with a distinctive linkage lens structure (note the change in scale).

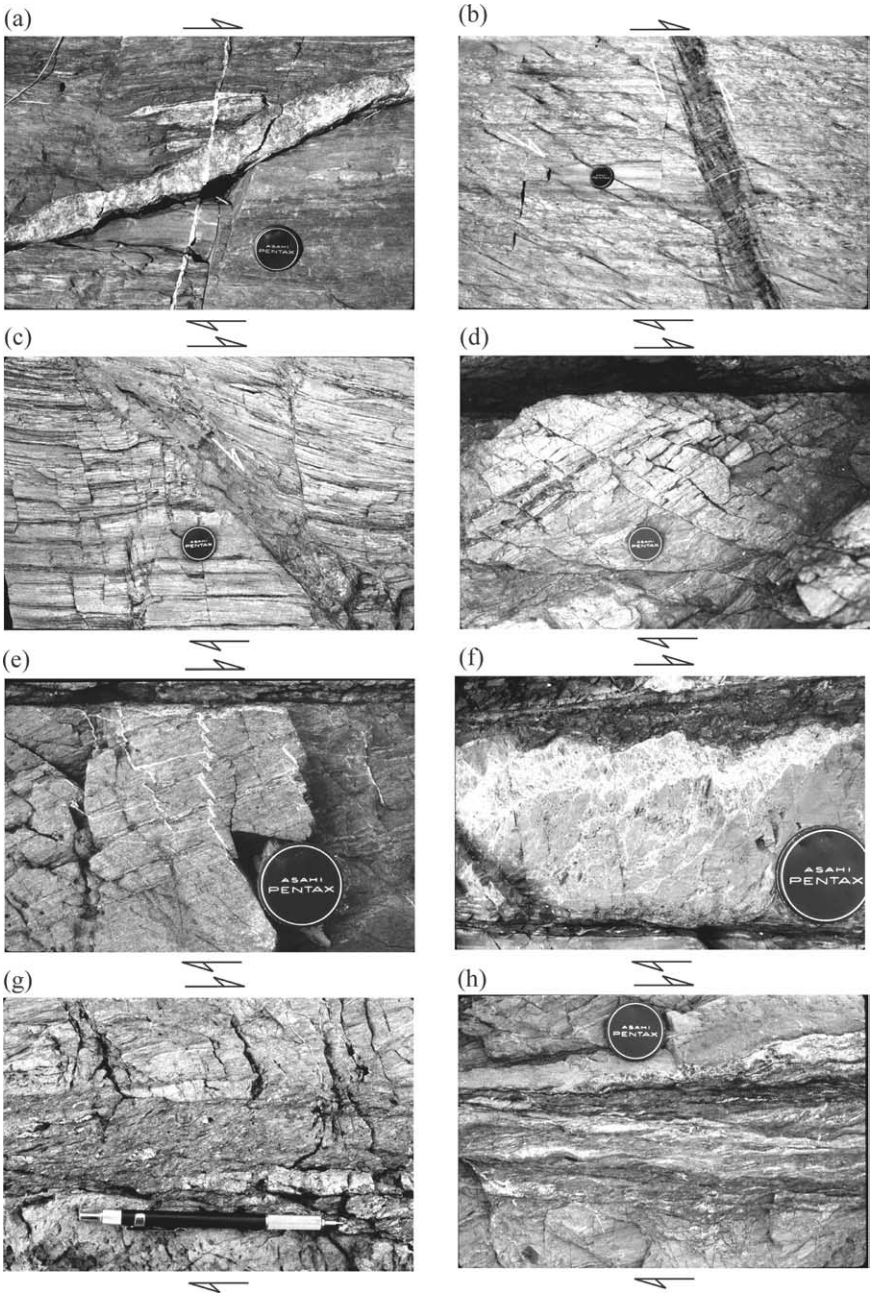

Fig. 7. Outcrop-scale characteristics of dextral strike-slip in the Cape Elizabeth fault zones. (a) Reorientation of quartz veins by clockwise rotation due to progressive dextral shear with older, more-reoriented, elongated quartz vein cut by younger planar quartz vein showing only minimal clockwise rotation. (b) Conjugate geometry between low angle-to-shear dextral shear band fabrics (as R-shears) and a single higher angle-to-shear sinistral kink band (as an R′-shear). (c) TL-1 fault zone structure showing offset and drag of local host rock layering against the pseudotachylyte-bearing main fault core zone with damage zone fracturing in the wall rocks. (d) Splay faults at the trailing end of an adhesive wear structure along the RI fault core zone. (e) Flanking quartz vein cut by later slip adjacent to the RI fault core zone. (f) Local silicified breccia zone adjacent to a fault segment in the RI fault zone. (g) 5-cm-wide obliquely-foliated dextral cataclastic core zone with recognizable clasts from the RI fault zone. (h) Larger, higher displacement core zone with more strongly-developed foliation. Arrows indicate dextral shear across each photograph. For (d)–(f) the main fault core zone runs across the top of each image. The lens cap is 5.5 cm in diameter and the pencil is 14 cm long.

Pseudotachylyte is recognized in only a few places within these core zones as millimeter-wide fault-parallel veins of very fine-grained dark gray material, commonly with tapered orthogonal injection veins extending only a few millimeters into the adjoining fault wall. In thin section the pseudotachylyte is found to contain rounded clasts (Fig. 8b), and cuspate boundaries with the wall rocks due to contact melting effects (Fig. 8d), as well as flow layering within the fault veins and larger reservoir structures.

Foliated cataclasites (Chester et al., 1985; Chester and Logan, 1986) are also commonly developed within the larger, more evolved fault segments at Richmond Island through clast rotation, clast alignment, pressure solution and cataclastic flow. The development of obliquely foliated

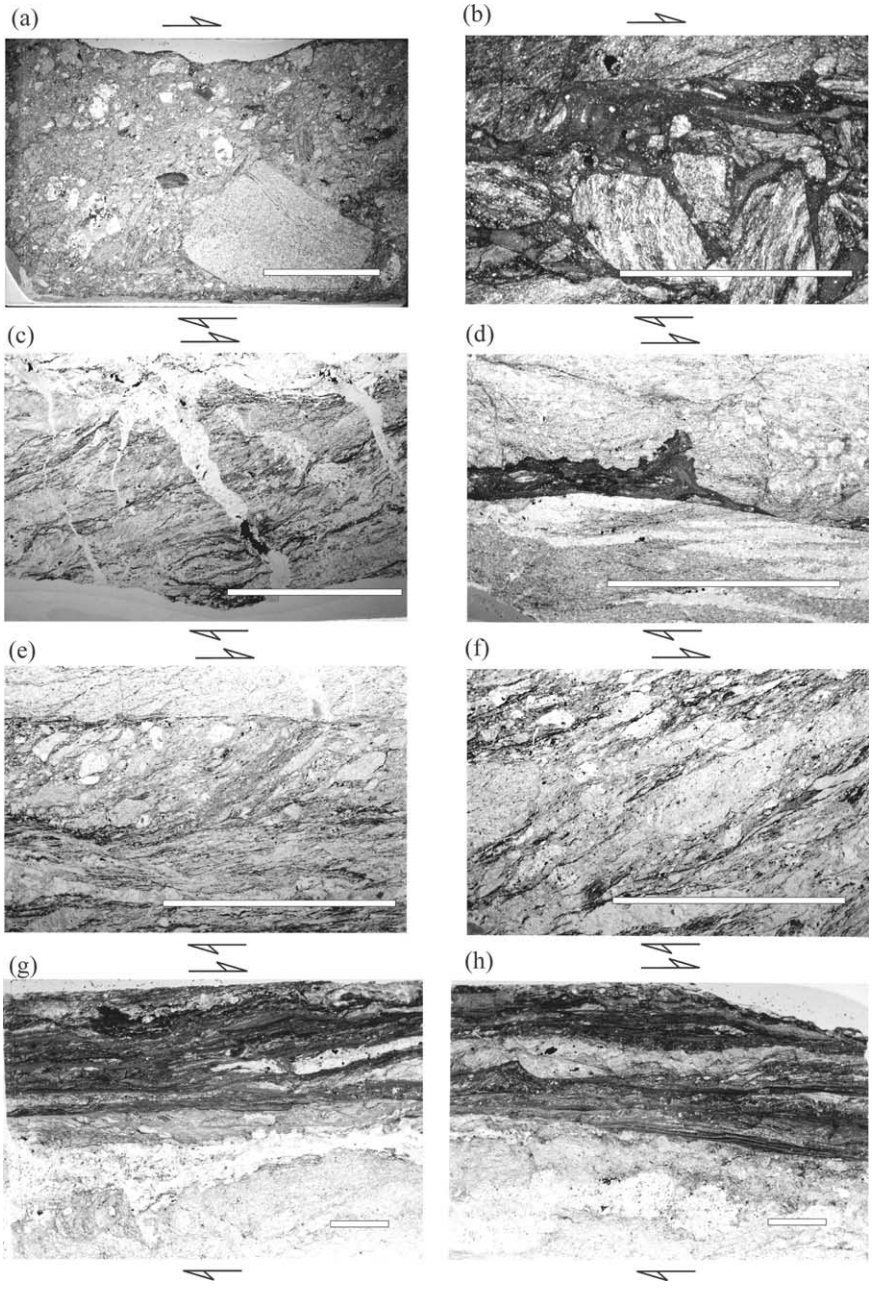

Fig. 8. Photomicrographs of dextral strike-slip fault rocks in thin section from the Cape Elizabeth fault zones. (a) Coarse-grained dilation breccia cemented with calcite and minor quartz from a pull-apart breccia structure in the TL-2 fault zone. (b) Coarse-grained dilation breccia with pseudotachylyte matrix from the Two Lights exposures. Note the rounded shapes to the included clasts due to resorption and thermal spalling. (c) Quartz veins and silicification adjacent to a segment of the RI fault zone. (d) Pseudotachylyte fault vein from the Two Lights fault zones showing internal flow layering and a cuspate resorption contact with the adjacent host rock. (e) A 0.5-cm-wide obliquely-foliated cataclasite zone in part of the RI fault zone. Several of the fragments within the cataclasite zone are finer grained cataclasite from earlier faulting episodes. (f) Obliquely-foliated cataclasite texture with foliation surfaces as solution planes from the RI fault zone. (g) and (h) Two contiguous thin sections of the TL-1 fault zone, showing the dark laminated core with reworked quartz lenses. Arrows indicate dextral shear across each photomicrograph. White bars = 1 cm.

cataclasite (Fig. 8e and f) leads to laminated core formation (Fig. 8g and h) with fabric rotation and enhanced pressure solution punctuated by frictional sliding and renewed cataclasis. Repetitive cycles of ultracataclasis and friction melting along with this cataclastic flow, pressure solution and fabric rotation have produced distinctive fault-parallel laminations within the narrow highly-strained core zone layers.

The presence of pseudotachylyte within these narrow higher strain core zones shows that some of these fault materials were produced during the rapid coseismic slip phase of the earthquake cycle. The accompanying cataclastic flow and solution creep associated with the laminated core zones represent a history of paleo-seismic activity (Knipe, 1989; Sibson, 1989; Gratier and Gamond, 1990) preserved along these fault zones.

4.4. Initial en échelon segmentation

An initial en échelon segmentation structure can be recognized within many of the Two Lights fault zones with segments ~35–50 m long although this is quite variable. Left-stepping geometries have stepover widths up to ~40 m with overlaps of up to ~20 m. In the TL-2 fault zone, one of the early R-shears can be recognized as a 35-m-long segment with an isolated horsetail termination that has been truncated and abandoned by P-shear linkage. Many of these early segments are, in turn, made up of their own smaller scale segments ~2–3 m long. The larger Richmond Island fault zone also has an initial en échelon structure with three distinct segments, ~400–500 m long, with stepover widths of 10–40 m and overlaps of ~10–100 m. Recognition of this early en échelon geometry is key in reconstructing fault zone evolution.

4.5. Terminations

The isolated ends of fault segments in these exposures typically terminate in arrays of quartz–ankerite veins oblique to the adjoining strike-slip fault segments (Fig. 9d and e) in a horsetail configuration (after Granier, 1985). Individual veins in these terminations are up to 1 m long with dozens of veins in individual termination arrays. A few composite structures (Fig. 9b and c) show a P-shear splay on the contractional side of the termination with a horsetail array on the extensional side of the termination. Larger-scale terminations with fractures several meters long are developed in the TL-1 fault zone (Fig. 6c) at the ends of two main fault segments at a 40 m left step in the TL-1 array.

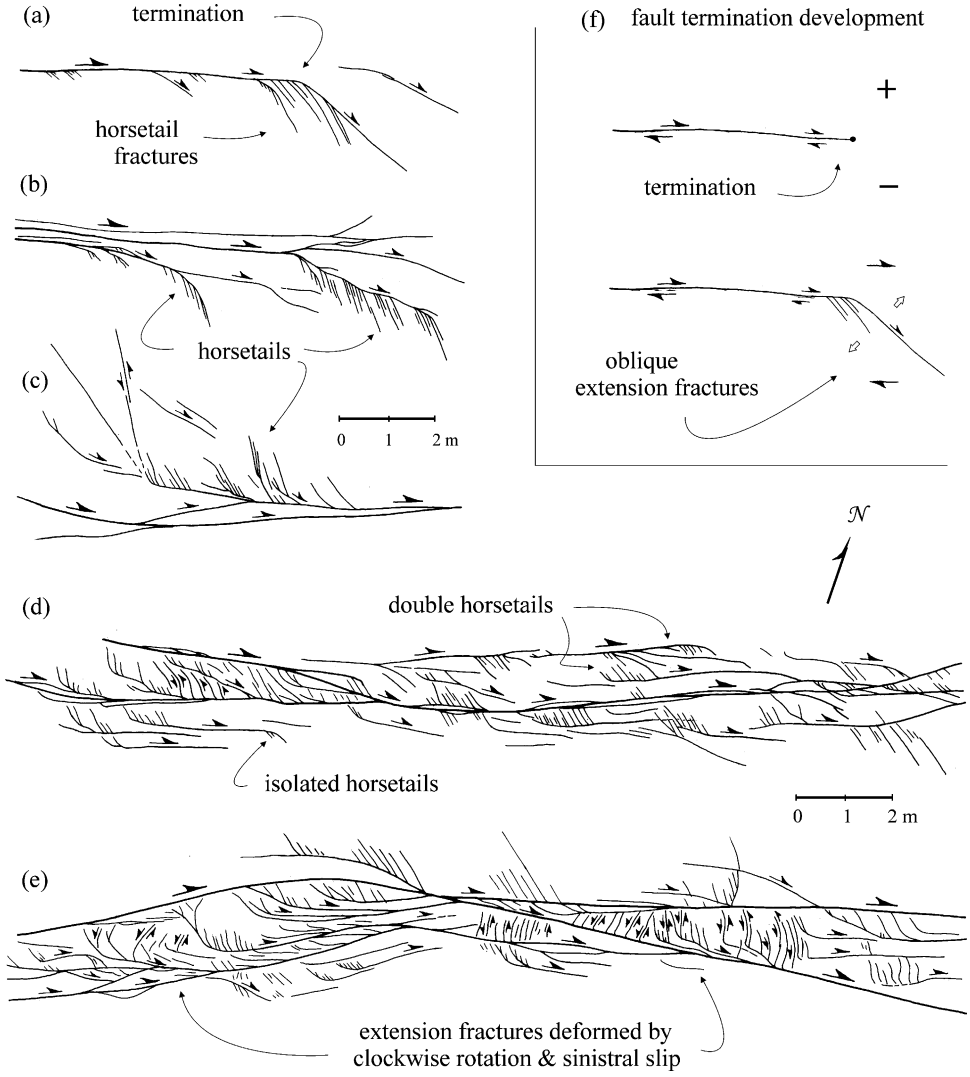

Fig. 9. Maps of fault terminations with oblique extension fractures. (a) Horsetail termination from the TL-2 fault zone. (b) Fringe terminations suggesting successive positions of fault tip. (c) Complex termination showing dextral and high-angle sinistral fault splays with contractional P-shears on the opposing side. (d) Extensional linkages that developed as isolated or paired, linking termination arrays. (e) Modification of extensional linkages by forward (clockwise) rotation and induced antithetic (sinistral) slip. (f) The development of fault terminations in relation to the contractional (+) and extensional (−) sides of a strike-slip fault tip and the formation of oblique extension fractures in horsetail splays.

4.6. Linkages

The initial en échelon geometry creates step-over zones between the ends of adjoining fault segments. The rock within these step-over zones must deform in order to accommodate continued displacement that leads to the formation of linking faults and the evolution of a through-going fault zone. The step-over zones develop in contractional and extensional styles that depend on the sense of slip and stepping direction of the en échelon fault segments. Dextral en échelon R-shears, as seen in these exposures, develop predominantly left-steps and contractional linkages.

4.6.1. Contractional linkages

The linkage of adjacent fault segments in left-stepping arrays (Fig. 10) is typically through the development of P-shear splay faults that are considered contractional because they accommodate fault parallel shortening as shearing proceeds. Multiple linking P-shears may create fault-bound lens geometries known as strike-slip duplexes (Woodcock and Fischer, 1986; Swanson, 1988; Cruikshank et al., 1991), where multiple closely-spaced splays form elongate horses imbricated between overlapping en échelon segments (Fig. 10b and d). Internal deformation within duplexes takes the form of multiple P-shears and P′-shears in the form of high-angle sinistral kink-bands (Fig. 10f). The formation of P-shear linkages will also isolate and abandon the outer sections of terminated segments in the initial array, as can be seen in Fig. 10a, b and d as well as on the larger-scale in the TL-2 fault zone (Fig. 8). Deformation of the bounding fault surfaces by slip along the linking P-shears can be seen in Fig. 10b, similar to deformation of roof thrusts in typical dip-slip duplexes (Boyer and Elliott, 1982) or in Fig. 10c where the overall configuration is equivalent to 'antiformal stacking' commonly developed in thrust complexes (Boyer and Elliott, 1982). For en échelon faults with significant overlap and multiple linkages

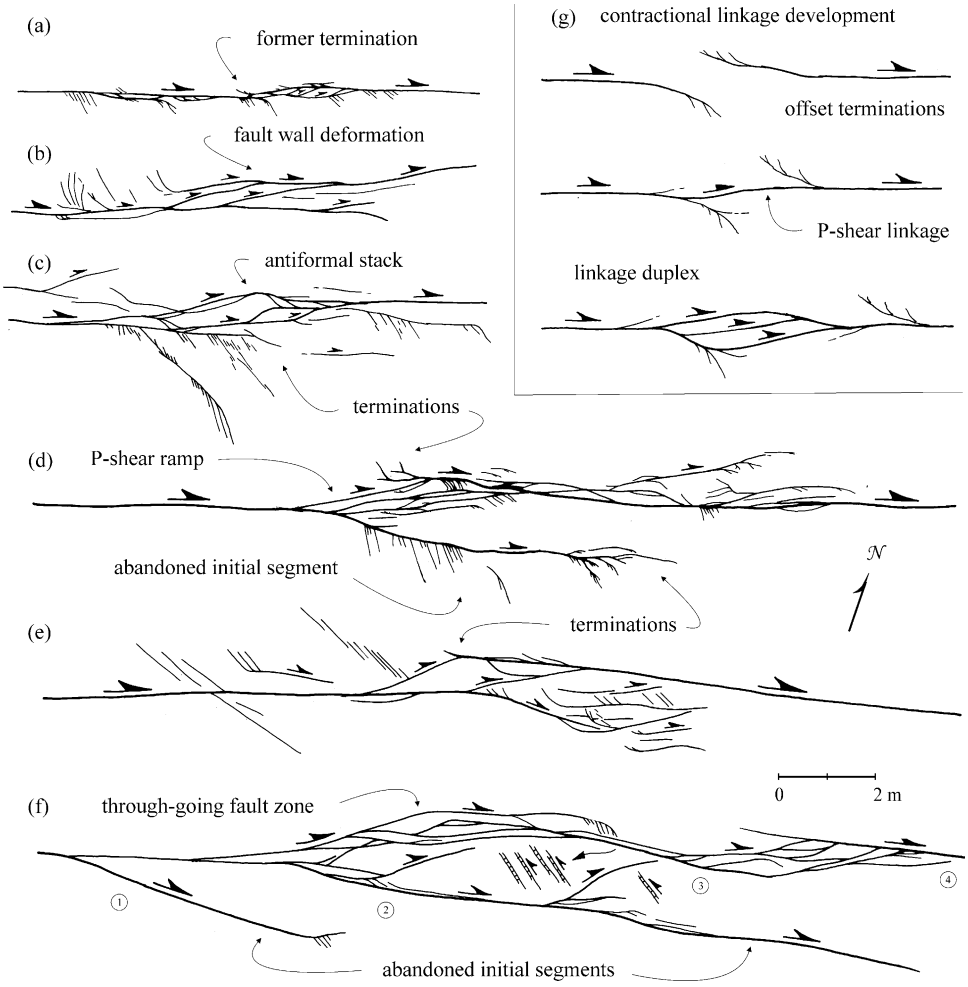

Fig. 10. Maps of contractional P-shear linkages between left-stepping faults. (a) Small-scale linking duplex that isolates the ends of initial en échelon segments marked by horsetail terminations. (b) P-shear imbrication showing deformation of 'upper' fault surface during displacement. (c) Complex imbrication at an en échelon offset that resembles antiformal stacking, common in thrust sequences. (d) Multiple slip surfaces developed during P-shear linkage that isolated former segment terminations. (e) P-shear imbrication and development of a contractional duplex upon linkage. (f) Through-going fault zone that links across four (numbered) en échelon fault segments (ladder symbols represent antithetic R′ kink bands). (g) Typical development and evolution of contractional linkages and linkage duplexes from stepping en échelon fault segments.

the resulting linkage duplex is typically an asymmetric fault lens (Fig. 10a and e) with similar P-shear splay faults at both ends.

Linkages across contractional stepovers that utilize antithetic minor faults at high angles to the bounding faults are less common. Such contractional linking structures have been described by McGarr et al. (1979), Hedgecoxe and Johnson (1986), Davis (1996), and Flodin and Aydin (2004). Continued displacement in these zones is accommodated by block rotation with antithetic slip along the intervening high angle minor faults. This can be seen in the Cape Elizabeth exposures as linking high angle R′ shears or kink bands in contractional stepovers and in the clockwise rotation of oblique extension fractures with increasing antithetic slip common in the TL-3 fault zone (Fig. 9d and e).

4.6.2. Extensional linkages

The dominant left-stepping geometry of the initial en échelon segments precludes the right-stepping dextral fault segments needed to form extensional linkages. Fault interaction within a wide complex zone of dextral shear may yield the required stepping geometries for extensional linkages but they are only locally developed in the exposed fault zones, particularly in the TL-2 and TL-3 structures (Fig. 9). Oblique fractures form as relays between the en échelon fault segments and, in some cases, represent the interaction of two opposing extensional horsetail termination arrays (after Granier, 1985), or zones of displacement transfer between active slip patches along adjacent fault surfaces as described by Martel and Pollard (1989). Similar extensional linkages have been described by Cruikshank et al. (1990) for faulted joints in sandstone, in experimental shear of offset cracks by Lin and Logan (1991) and in regional fault zones by Sibson (1985, 1990). Gamond (1983, 1987) also described small-scale examples of extensional linkages and associated mineralization in granite. In the TL-2 fault zone, extensional linkages occur in the wider spaced step-over zone where non-linking P-shear splays across this intact step-over yield the needed right-stepping geometries.

4.7. Fault zone modifications

Once the initial en échelon segments have linked through connecting splay faults the resulting through-going zone has an irregular trace consisting of alternating R-shear and P-shear segments. The differences in orientation of these segments relative to the overall slip direction means that the P-shear linkages are in restraining orientations for continued displacements. Further fault zone evolution involves the modification of these restraining sections through both abrasive and adhesive wear to form a more planar through-going fault zone. Abrasive wear plays an integral role in the production of the cataclastic core zone of the faults. Adhesive wear (Swanson, 1989, 2005), referred to as scuffing, seizing or galling in the engineering literature (Rabinowicz, 1965; Bowman and Stachowiak, 1996), contributes significantly to the outcrop-scale lens structure of the through-going zones.

Wall rock isolated by splay faults to form asymmetric fault-bounded lenses and slabs are referred to as sidewall ripouts (Swanson, 1989, 2005). A distinctive 10-m-long slab ripout in the TL-1 fault zone (Fig. 6a) may have developed along a restraining P-shear linkage that formed across the initial array. The most prominent feature in the TL-3 fault zone (Fig. 6c) is a series of nested ripouts that distort the main fault surface. The larger RI fault zone (Fig. 6d) has numerous ripout lenses distributed throughout the structure but most are concentrated along the dominant P-shear linkage contributing to the overall anastamosing structure of this part of the residual through-going zone.

5. Fault sequencing and the linkage-growth model for fault zone evolution

Distinctive structures and geometries within the Two Lights and Richmond Island faults can be related to different stages in a linkage-growth model for fault zone evolution. In this model, larger faults coalesce from initial en échelon R-shear arrays through the development of P-shear linkages to create a through-going fault zone. This style of fault zone evolution where linking structures evolve from en échelon shear fractures (e.g. Vermilye and Scholz, 1999; Ahlgren, 2001) is just one of several models available for fault zone development. Alternate models include R-shear en échelon arrays with antithetic R′-shear linkages (McGarr et al., 1979; Hedgecoxe and Johnson, 1986; Davis, 1996) as well as forming fault zones from preexisting joints or joint arrays (Martel and Pollard, 1989; Cruikshank et al., 1990; Mollema and Antonellini, 1999; Pachell and Evans, 2002; Flodin and Aydin, 2004), from en échelon veins (Willemse et al., 1997; Kelly et al., 1998), in conjugate fault networks (Kelly et al., 1998; Flodin and Aydin, 2004) and from extension cracks in experimental studies (Cox and Scholz, 1988).

5.1. Fault growth by P-shear linkage of initial en échelon segments

The sequences of faults illustrated in Figs. 11 and 12 for the Richmond Island (RI) and Two Lights (TL-2) fault zones are depicted in a three-stage model, from the interpreted initial en échelon strike-slip fault segments, through P-shear linkage structures to a final through-going fault zone as mapped in these exposures. The RI fault zone has greater displacement and represents a later stage in fault zone evolution than the smaller displacement Two Lights faults and thus has a more complex structure.

The RI fault zone (Fig. 11) displays an initial en échelon structure with three distinct segments of 400–500+ m length along the main zone of faulting with stepover widths of ~10 and 40 m. Multiple P-shear linkages have isolated two lenses of host rock as contractional duplexes. The smaller (60 m long, 10 m wide) linkage duplex at the western end of the mapped fault has multiple internal imbrication that creates a series of contractional horses. The larger (300 m long, 40 m wide) linkage duplex has few internal structures but has

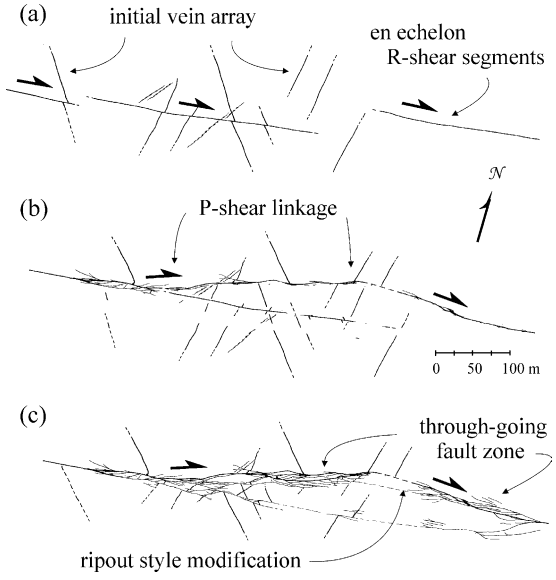

Fig. 11. RI fault zone reconstruction. (a) Three initial en échelon segments and preexisting quartz veins. (b) P-shear linkage through prominent P-shear ramp. (c) Through-going fault zone with imbrication to form larger linkage lens or duplex with ~40 m of displacement.

accommodated most of the displacement along its northern bounding P-shears. In the central section of the map, several distinctive curved splays merge and extend across an intertidal area (dashed in Fig. 8d) to define a 100-m-long ripout structure. This larger ripout appears to have sheared off the restraining P-shear/R-shear intersection of the larger linkage duplex.

The reconstruction of the TL-2 fault zone (Fig. 12) is based on a well-constrained sequence, with initial en échelon segments that link to a through-going fault. These initial segments are ~35–50 m long with stepover widths up to ~6 m. One of these initial R-shear segments (examined in more detail below) is 35 m long with a single horsetail termination now truncated and abandoned by P-shear linkage. The exposed fault zone contains several different P-shear linkage structures on a variety of scales across variable width steps in this complex en échelon zone. Several of the linkages on the western end of the mapped structure merge to bring the through-going slip surface right across the initial array. The larger (6 m wide) stepover on the eastern end of the mapped structure had not been completely breached and contains several oblique P shears that have failed to connect across the gap.

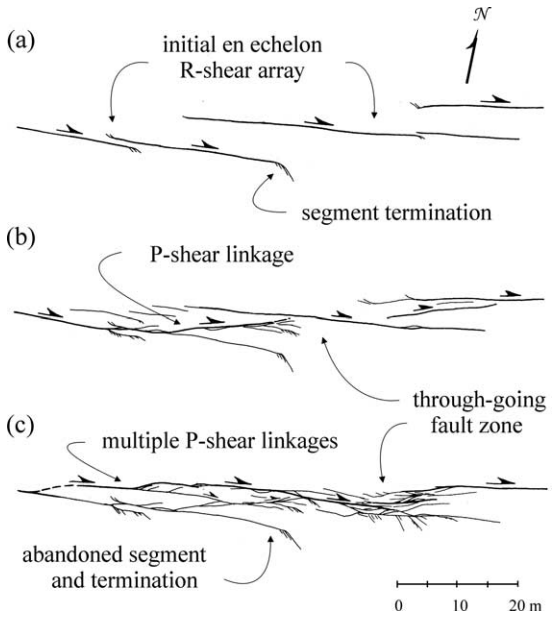

Fig. 12. TL-2 fault zone reconstruction. (a) Initial en échelon R-shears. (b) P-shear linkages isolate the outer terminated segments of the initial oblique R-shears. (c) Through-going fault zone with ~5 m of displacement.

The dextral strike-slip fault zones in the Cape Elizabeth exposures are themselves part of a 10-km-long zone of oblique en échelon faults (Fig. 2b). Each kilometer-long fault within the zone had reached the stage of through-going fault zone development, with the linkage of smaller-scale R-shear fault segments in the 10–100 m scale range. These segments were formed from even smaller-scale segments in the 2–8 m range. The P-shear linkages in these fault zones allowed growth to kilometer or near kilometer lengths and increased total displacements. Fig. 13 illustrates the observed fault geometries in the Cape Elizabeth exposures at various scales from the 1 m to 10 km field of view. The 1 m view shows the linked structure of the truncated initial fault segment within the TL-2 fault zone. The 100 m view shows the complete linkage structure of the through-going TL-2 fault zone. Note that this through-going fault geometry persists through the 100 m view, but is absent from the 1 and 10 km views that follow. Continued displacements on the kilometer-long Cape Elizabeth fault zones could have led to even larger-scale linkage structures on what could have become a major regional brittle crustal fault zone accommodating continued regional strike-slip deformation.

6. Discussion

6.1. Displacement/length relationships

Detailed mapping of a 22 m section of the TL-2 initial segment and termination described above also reveals a smaller-scale internal lens and splay structure. Linked en échelon segments on a smaller scale remain in the residual geometry of this 35 m long 'initial' segment. Cross-cutting preexisting deformed quartz veins and boudin strings allowed displacement/length (d/l) profiling along this abandoned segment (Fig. 14). This can pinpoint sections of low d/l values typical for breached or linked offsets (Ellis and Dunlap, 1988; Peacock, 1991; Pachell and Evans, 2002) that are now exposed as terminated splay faults or asymmetric lenses. This 'initial' 35-m-long fault segment has thus formed from its own smaller scale en échelon segments with segment lengths on the order of ~2–8 m as indicated by the spacing of displacement minima in the Fig. 14b profile.

A maximum displacement/length (d_{max}/l) ratio reflects the elastic strain limit for the host rock under deformation (Muraoka and Kamata, 1983) before linkage structures develop. Typical d_{max}/l ratios for isolated small-scale normal

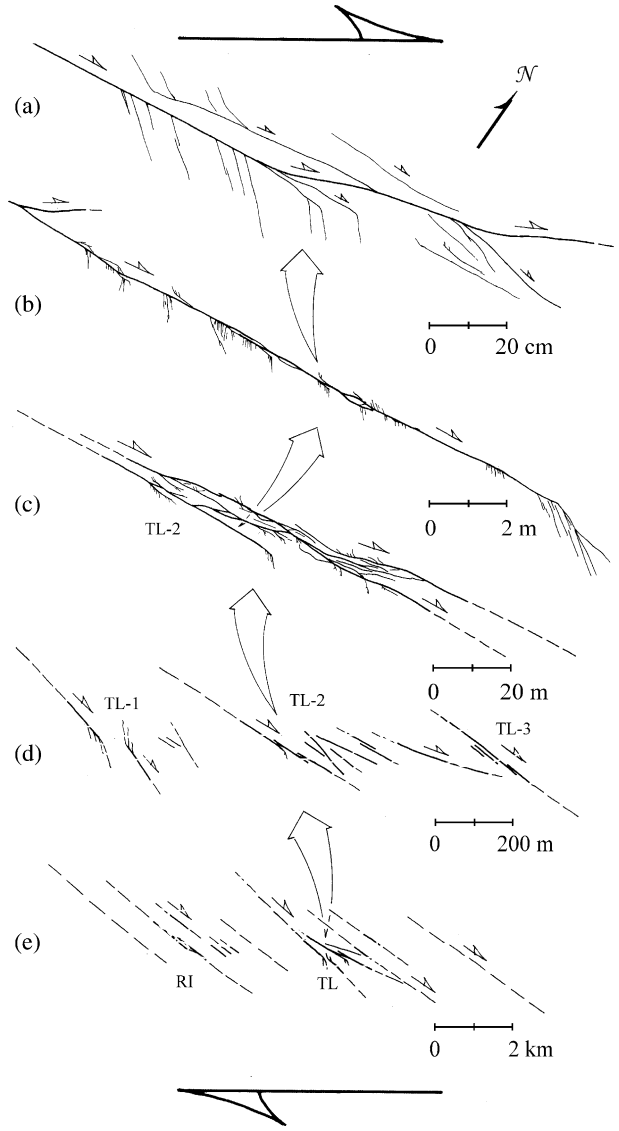

Fig. 13. Multi-scale views of the Cape Elizabeth fault zones. (a) 1 m view of the internal structure of an initial en échelon segment in the TL-2 fault zone showing its own internal linked segmentation structure. (b) 10 m view of the full length of the abandoned R-shear section (see Fig. 15a) with horsetail termination cutoff by P-shear linkage. (c) 100 m view of the linkage-growth structure of TL-2 fault zone with P-shear linkages across en échelon R-shear segments. (d) 1 km view of the full Two Lights outcrop exposure of the TL-1, TL-2, and TL-3 faults from left to right. (e) 10 km view of the full Cape Elizabeth exposures with the TL and RI fault zones. Gray lines in (d) and (e) represent outcrop outline and shoreline, respectively.

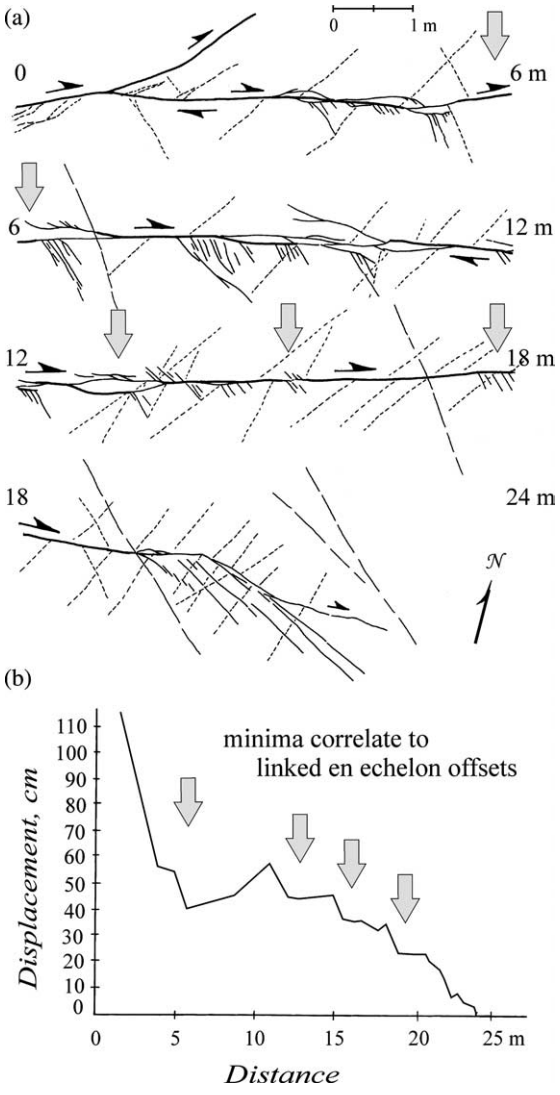

Fig. 14. Internal structure of the TL-2 fault zone. (a) Detailed map of a continuous 22 m section of the 35 m long initial fault segment in the TL-2 fault zone where abandoned by P-shear linkage showing internal structure and termination. (b) Displacement/distance profile suggests early segmentation within the abandoned TL-2 segment. Arrows indicate displacement minima and their positions along the mapped fault as possible linked offsets in an earlier, smaller-scale, en échelon array of strike-slip segments in the ~2–8 m length range. Short dashed lines represent early deformed quartz veins offset by faults. Long dashed lines are later stage, planar quartz veins that cross-cut the faults.

faults in sedimentary rocks have been found to range from 0.002 to 0.04 (Muraoka and Kamata, 1983), with an average of ~0.01. Ratios of ~0.37–0.004 and an average of 0.021 were reported for strike-slip faults in sandstone/shale turbidities (Peacock, 1991). Dawers and Anders (1995) reported d_{max}/l values of 0.009–0.014 for single segment normal faults in a 7-km-long fault zone. The longer fault zone developed through linkage of segments and yielded a d_{max}/l value for the zone of 0.013. Lithological variations may account for most of the range of values, with incompetent units allowing higher strain gradients at the fault tips and higher d_{max}/l ratios than more competent units (Muraoka and Kamata, 1983; Peacock, 1991). Many of the lower d_{max}/l ratios may be from just-linked faults ready to accommodate additional displacement (Cartwright et al., 1995).

An isolated 50-m-long dextral fault segment in the Two Lights exposure with measured displacement of 0.75 m gives a d_{max}/l ratio of 0.015 and the early terminated segment described above from the TL-2 fault zone gives a d_{max}/l ratio of 0.034. Using an average estimate of 0.025 for the d_{max}/l ratio in these lithologies, the Richmond Island fault zone with total (maximum?) displacements of ~40 m must be at least 1.6 km long. Likewise, total (maximum?) displacements

of ~5 m for the Two Lights fault zones suggest likely total fault zone lengths of ~0.2 km.

Given the way in which these fault zones have evolved through the development of a progression of multi-scale linkages, the total fault length and d_{max}/l ratios must have also developed in a step-wise fashion (Cartwright et al., 1995; Mansfield and Cartwright, 2001). Interaction between adjacent fault segments would build higher strain gradients at the fault tips (Peacock, 1991) to the limiting d_{max}/l ratio and lead to eventual linkage. Linkage abruptly increases total fault length, temporarily decreasing the d_{max}/l ratio, allowing the accumulation of additional displacements and building toward the limiting d_{max}/l ratio characteristic for that particular lithology.

6.2. Fault length distribution

Length–frequency diagrams for fault segments within each of the fault zones illustrate the length distributions within the fault segment population developed during fault zone evolution (Fig. 15). Straight line segments on log–log plots of cumulative fault length imply a power-law scaling where the negative slope of the line (as the exponent of the power-law equation) is referred to as the fractal dimension (Mansfield and Cartwright, 2001; Flodin and Aydin, 2004). Power-law exponents for natural fault populations reported by Cladouhos and Marrett (1996) from a variety of locations and scale ranges were found to vary between 0.67 and 2.07. Multiple generations of faults in a single location (Flodin and Aydin, 2004) show a range of power-law exponents from 1.2 to 1.68 but only for a restricted scale range of 20–110 m fault lengths. The length–frequency diagrams for the TL and RI fault zone segments all show linear middle sections with an average negative slope or power-law exponent of 1.65 over an average scale range of ~1–15 m fault lengths.

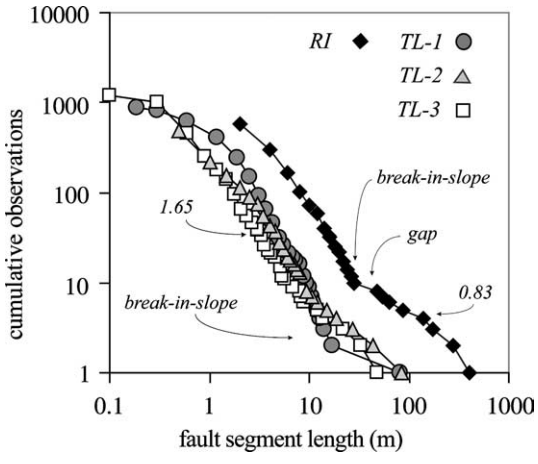

Fig. 15. Length–frequency diagram for fault segments in the Cape Elizabeth fault zones. The linear middle sections of all the plots have similar slopes that give an average power-law exponent of 1.65 with power-law behavior for fault zone development in the scale range of ~1–15 m. A gap and break in slope in the lower part of the curves reflects the onset of significant fault growth through linkage that gives a lower average power-law exponent of 0.83 for fault segments greater than ~15 m.

The change in slope that commonly occurs at the left side of these length–frequency diagrams (Fig. 15) likely reflects the resolution of the mapping technique as a sampling bias where the more numerous smaller faults are progressively more difficult to represent (Mansfield and Cartwright, 2001; Flodin and Aydin, 2004). The right-hand side of many diagrams often involves a steepening of the lower part of the curve referred to as 'rollover' (Cladouhos and Marrett, 1996). This can be attributed to recording apparent fault length values where the longer fault lengths are underestimated due to the finite width of the available exposure. However, the length–frequency diagrams from the Cape Elizabeth fault zones show a distinctive break in slope and a *flattening* of the lower portion of the graph before the rollover for longer fault lengths (Fig. 15; TL-3 and RI fault zones in particular). The lower sections of the Cape Elizabeth diagrams have an average power-law exponent of only 0.83 for average fault segment lengths of ~15 m and greater (compared with an average power-law exponent of 1.65 for ~1–15 m fault lengths in the middle sections of the diagrams). Individually, this threshold fault length at the break-in-slope varies between the different fault zones. The fault length threshold for the TL fault zones varies from 8 to 17 m while the value for the larger and higher displacement RI fault zone is at ~28 m.

Such breaks in slope as well as associated gaps (Fig. 15; TL-1, TL-2 and RI fault zones) in the length–frequency diagrams represent the abrupt development of longer lengths during linkage that is reflected in a decrease in the power-law exponent or fractal dimension for the longer fault segment populations (Cladouhos and Marrett, 1996; Mansfield and Cartwright, 2001). Such a break in slope (and decrease in the power-law exponent) for longer fault lengths can be seen in experimental data (Cladouhos and Marrett, 1996) and is apparent in only a few of the reported fault populations (Flodin and Aydin, 2004; Fig. 15). As suggested by Flodin and Aydin (2004) this implies that the power-law behavior of developing fault populations is limited to restricted scale ranges. Several different power-law functions develop for the different scale ranges of the evolving population as a type of multi-fractal behavior (Cowie et al., 1995). The Cape Elizabeth faults display early power-law behavior over an apparent initial scale range of ~1–15 m with fault growth perhaps dominated by propagation. This early development corresponds to the formation of most of the damage zone structures and early segments associated with these fault zones. Later linkage-dominated growth and localization to a longer through-going fault zone results in a switch to a lower slope and decreased power-law exponent for the evolving fault segment population. This correlates to the development of the fault core zone and the accumulation of the bulk of the displacement.

6.3. Fluid involvement in faulting

The interaction between fluids and fracturing during the earthquake cycle is a complex process and, in the Cape Elizabeth exposures, led to complicated field relationships between faults and veins. The geometry and cross-cutting

relationships of these faults and veins reflect sequential and cyclic changes in fluid pressure, differential stress and stress orientation that developed as regional shearing progressed and fault zones initiated and evolved with increasing displacements through multiple earthquake cycles.

The intermittent emplacement of vertical veins orthogonal to the shear zone boundaries reflects strain partitioning during early dextral shear and serves as a mechanism to relieve fluid pressure associated with regional transpression. Rising pore fluids and increasing fluid pressures were driven by localized crustal thickening and subsequent dehydration in the lower crust. In the Cape Elizabeth exposures, the gently-inclined orientation of the phyllite–quartzite host rock layering created a barrier to vertical fluid flow capable of building local fluid pressures that, in turn, triggered intermittent shear and extensional fracturing. The Cape Elizabeth strike-slip faults also have steep to moderate NW dips and could, themselves, have created a barrier to upward fluid flow similar to high-angle reverse faults (Cox, 1995; Robert et al., 1995; Nguyen et al., 1998), and hence acted as valves during their displacement history. The emplacement of veins throughout the bulk of the ductile shearing in these exposures (Fig. 16a and b) indicates extensional fracturing as the active valving mechanism during most of the transpression.

The association of faults and discrete vein arrays seen here (Fig. 16c–e) is similar to vein relationships developed during fault valve behavior on reverse faults in contractional and transpressional environments from Canada and Australia (Cox, 1995; Robert et al., 1995; Nguyen et al., 1998). All of these fault localities show similar vein lengths (up to 50 m), vein thicknesses (up to ~1 m) and are associated with similar length faults (up to ~1 km) with similar displacements (up to 10s of meters). All of these fault exposures show distinct vein arrays associated with most fault segments where there is a decrease in vein intensity, continuity and thickness away from the faults (Cox, 1995) as can be seen in the Cape Elizabeth exposures (Fig. 6c). Robert et al. (1995) note the spatial association of veins and faults and conclude that the fault zones must have been the source of the pressured fluids involved in the veining event.

Nguyen et al. (1998) also note that early brittle faulting accompanied by ductile deformation and foliation development changed to brittle faulting with extensional fracturing as shearing continued. This extensional failure formed flanking vein arrays that included extensional veins and conjugate sets of 'hybrid extensional shear veins' or 'oblique extensional veins' (Poulsen and Robert, 1989; Nguyen et al., 1998) with typically small dihedral angles. Similar vein arrays and late conjugate small dihedral angle strike-slip faults have developed in the Cape Elizabeth exposures (Fig. 6a) where the associated elongation reflects continued strain partitioning during regional transpression.

Such a change in deformation style from early ductile shearing and veining (Fig. 16a and b) to brittle faulting and veining (Fig. 16c–e) reflects the erosional unroofing and progressive strain hardening characteristic of transpressional deformation zones. Low differential stresses and rising fluid pressures during early ductile shearing at greater depths likely drove repeated extensional fracturing and vein development that resulted in fluid flow and valving of local fluid pressure. The later transition to brittle faulting as the valving mechanism correlates to more shallow crustal levels where strain hardening increased the level of differential stress prior to failure. Increasing fluid pressure under these higher differential stress conditions triggered the repeated brittle shear failure in

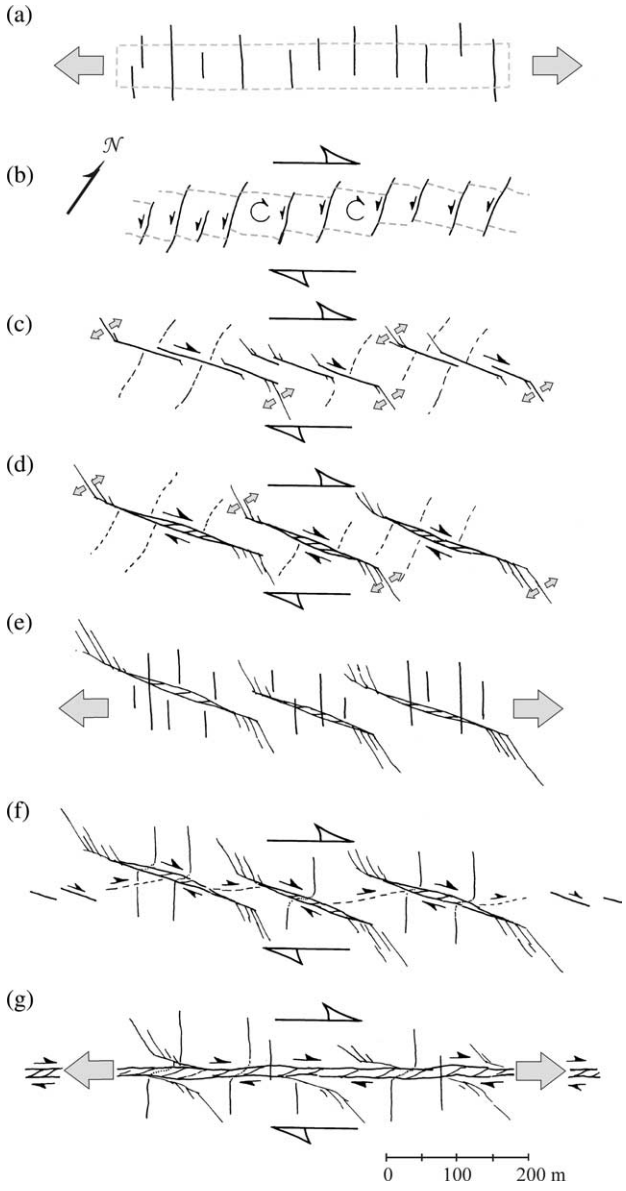

Fig. 16. Sequence of veins and faults due to progressive shearing in the Cape Elizabeth fault zone exposures. (a) Extensional valving and formation of initially orthogonal-to-shear quartz vein arrays during strain partitioning of transpressional deformation. (b) Continued shearing results in clockwise rotation of rocks and structures with antithetic vein-parallel sinistral slip. (c) Strain hardening during shear forms en échelon dextral R-shear fault zones, with each zone made up of their own smaller-scale en échelon segments. (d) Linkage of early en échelon segments to form through-going fault zones. (e) Cataclastic flow, compaction and fluid expulsion results in formation of adjoining quartz vein arrays. (f) Continued shearing along fault zones deforms earlier veins and promotes larger-scale P-shear linkages. (g) Final stage through-going fault zone with complex history of syntectonic veining.

the fault zones where faulting and cataclasis allowed fluid flow, relieved local fluid pressures and led to silicification of the cataclastic fault materials.

During the post-seismic period of creep deformation under relatively low differential stress, compaction, pressure solution and cataclastic flow along the fault zone are accompanied by a progressive decrease in porosity and permeability during core zone formation. This will expel fluid (Sleep and Blanpied, 1994) and eventually seal off the fault core zone forcing fluid flow through the flanking damage zone aureole (Evans et al., 1997). Both of these effects would contribute to the return of higher fluid pressures around the fault zones that, under low post-seismic differential stresses, would drive the formation of the late extensional veins associated with each of the fault zones. With continued displacement, initial core zone formation through cataclastic flow, pressure solution, fluid expulsion and wall rock veining (Fig. 16e) would be surpassed by further strain localization, laminar cataclastic flow and accumulating displacement within an established core structure that would cross-cut these earlier vein arrays (Fig. 16g).

7. Conclusions

The Two Lights and Richmond Island fault zones of Cape Elizabeth are part of a 10-km-long zone of en échelon R-shears related to regional dextral strike-slip deformation on the southeast flank of the Norumbega fault system. These kilometer-long R-shear segments show a sequence of development with increasing displacement from initial en échelon faulting through P-shear linkage, and structural duplexing. Fault zone modification processes of adhesive wear along the through-going faults were dominant mechanisms during continued displacement, contributing to a more planar anastamosing zone of bulk cataclastic flow. Shallow crustal fault rocks range from pseudotachylyte to cataclasite and can be related to a paleo-history of coseismic slip events. Through-going cataclastic fault zones typically develop obliquely-foliated to laminated cataclasite in well-developed core structures dominated by cataclastic flow related to interseismic creep. Compaction of the cataclasite during shear led to a decrease in porosity, increased pressure solution and fluid expulsion during fault core formation, which can be related to peripheral quartz veining at the outcrop scale. This fluid history coupled with a linkage-growth model implies that regional kilometer-scale fault zone evolution proceeded through a sequence of progressively larger-scale en échelon segments and linkages to form a series of fluid-expelling fault core zones and peripheral vein arrays as displacement accumulates. Linkage structures allow abrupt fault growth with a jump in overall fault length, which, in turn, will allow larger displacements on these now longer faults. The onset of linkage-dominated fault growth at $\sim$15 m fault lengths is reflected in the slope geometry of the length–frequency diagrams for the fault segment populations. The end result is to maintain fault geometry below a limiting maximum displacement/length ratio reflecting a maximum elastic fault-parallel strain characteristic for the host rock lithology.

Acknowledgements

Research for this project was supported by the U.S. Geological Survey, Department of the Interior under the National Earthquake Hazards Reduction Program, Award nos. 14-08-0001-Gl395, 14-08-0001-Gl702 and 14-08-0001-G2060 for l987, 1989 and 1991. The University of Southern Maine provided released time from academic duties in support of this project. Reviews and comments by David Peacock, Pierpaolo Guarnieri and Tom Blenkinsop helped to improve the manuscript. Thanks to Leo Algeo for assistance in plane tabling efforts at Richmond Island and to students in the Structural Geology class for help in analyzing the fault and vein arrays in these exposures.

References

Ahlgren, S.G., 2001. The nucleation and evolution of Riedel shear zones in deformation bands in porous sandstone. Journal of Structural Geology 23, 1203–1214.

Arboleya, M.L., Engelder, T., 1995. Concentrated slip zones with subsidiary shears: their development on three scales in the Cerro Brass fault zone, Appalachian Valley and Ridge. Journal of Structural Geology 17, 519–532.

Arch, J., Maltman, A.J., Knipe, R.J., 1988. Shear zone geometries in experimentally deformed clays: the influence of water content, strain rate and primary fabric. Journal of Structural Geology 10, 91–99.

Barka, A.A., Kadinsky-Cade, C., 1988. Strike-slip fault geometry in Turkey and its influence on earthquake activity. Tectonics 7, 663–684.

Bartlett, W.L., Friedman, M., Logan, J.M., 1981. Experimental folding and faulting of rocks under confining pressure. Part IX. Wrench faults in limestone layers. Tectonophysics 92, 667–686.

Bothner, W., Hussey, A.M., 1999. Norumbega Connections: Casco Bay, Maine to Massachusetts?. In: Ludman, A., West, D.P. (Eds.), Norumbega Fault System of the Northern Appalachians Boulder Colorado. Geological Society of America Special Paper 331, pp. 59–72.

Bowman, W.F., Stachowiak, G.W., 1996. A review of scuffing models. Tribology Letters 2, 113–131.

Boyer, S.E., Elliott, D., 1982. Thrust systems. American Association of Petroleum Geologists Bulletin 66, 239–267.

Cartwright, J.A., Trudgill, B.D., Mansfield, C.S., 1995. Fault growth by segment linkage: an explanation for scatter in maximum displacement and trace length data from Canyonlands Grabens SE Utah. Journal of Structural Geology 17, 1319–1326.

Chester, F.M., Logan, J.M., 1986. Implications for the mechanical properties of brittle faults from observation of the Punchbowl fault zone, California. Pure and Applied Geophysics 124, 79–106.

Chester, F.M., Friedman, M., Logan, J.M., 1985. Foliated cataclasites. Tectonophysics 93, 139–146.

Cladouhos, T.T., Marrett, R., 1996. Are fault growth and linkage models consistent with power-law distributions of fault length? Journal of Structural Geology 18, 281–293.

Cowie, P.A., Sornette, D., Vanneste, C., 1995. Multifractal scaling properties of a growing fault population. Geophysical Journal International 122, 457–469.

Cox, S.F., 1995. Faulting processes at high fluid pressures: an example of fault valve behavior from the Wattle Gully Fault, Victoria, Australia. Journal of Geophysical Research 100, 12841–12859.

Cox, S.J.D., Scholz, C.H., 1988. On the formation and growth of faults: an experimental study. Journal of Structural Geology 10, 413–430.

Cruikshank, K.M., Zhao, G., Johnson, A.M., 1990. Analysis of minor fractures associated with joints and faulted joints. Journal of Structural Geology 13, 865–886.

Cruikshank, K.M., Zhao, G., Johnson, A.M., 1991. Duplex structures connecting fault segments in Entrada Sandstone. Journal of Structural Geology 13, 1185–1196.

Davies, R.K., Pollard, D.D., 1986. Relations between left-lateral strike-slip faults and right-lateral monoclinal kink bands in granodiorite, Mt. Abbot quadrangle, Sierra Nevada, California. Pure Applied Geophysics 124, 177–201.

Davis, G.H., 1996. "Riedel relays" in deformation band shear zones, Colorado Plateau, Utah. Geological Society of America Abstracts with Programs 28, A-188.

Davis, G.H., Bump, A.P., Garcia, P.E., Ahlgren, S.G., 1999. Conjugate Riedel deformation band shear zones. Journal of Structural Geology 22, 169–190.

Dawers, N.H., Anders, M.H., 1995. Displacement–length scaling and fault linkage. Journal of Structural Geology 17, 607–614.

Dougherty, J.T., Lyons, J.B., 1980. Mesozoic erosion rates in northern New England. American Association of Petroleum Geologists Bulletin 91, 16–20.

Dunn, G.R., Lang, H.M., 1988. Low pressure metamorphism in the Orrs Island–Harpswell Neck area, Maine. Marine Sedimentation and Atlantic Geology 4, 257–266.

Ellis, M., Dunlap, W.J., 1988. Displacement variation along thrust faults: implications for the development of large faults. Journal of Structural Geology 10, 183–192.

Evans, J.P., Forster, C.B., Goddard, J.V., 1997. Permeability of fault-related rocks and implications for hydraulic structure of fault zones. Journal of Structural Geology 19, 1393–1404.

Flodin, E.A., Aydin, A., 2004. Evolution of a strike-slip fault network, Valley of Fire State Park, southern Nevada. Geological Society of America Bulletin 116, 42–59.

Gamond, J.F., 1983. Displacement features associated with fault zones: a comparison between observed examples and experimental models. Journal of Structural Geology 5, 33–45.

Gamond, J.F., 1987. Bridge structures as sense of displacement criteria in brittle fault zones. Journal of Structural Geology 9, 602–620.

Granier, T., 1985. Origin, damping and pattern of development of faults in granite. Tectonics 4, 7212–7227.

Gratier, J.P., Gamond, J.F., 1990. Transition between seismic and aseismic deformation in the upper crust. In: Knipe, R.J., Rutter, E.H. (Eds.), Deformation, Rheology and Tectonics. Geological Society Special Publication 54, pp. 461–473.

Grocott, J., 1981. Fracture geometry of pseudotachylyte generation zones: a study of shear fractures formed during seismic events. Journal of Structural Geology 3, 169–178.

Hedgecoxe, H.R., Johnson, B., 1986. Interaction between en echelon faults and formation of displacement transfer zones—examples from small fault systems in the Llano Uplift of central Texas. Geological Society of America Abstracts with Programs 71, 95–116.

Hickman, S., Sibson, R., Bruhn, R., 1995. Introduction to the special issue: mechanical involvement of fluids in faulting. Journal of Geophysical Research 100, 12831–12840.

Hussey, A.M., 1985. Bedrock geology of the Bath and Portland 2 degree map sheets. Maine Geological Survey Open File Report 85-87, 82.

Hussey, A.M., 1988. Lithotectonic stratigraphy, deformation, plutonism and metamorphism, Greater Casco Bay region, southwestern Maine. In: Tucker, R.D., Marvinney, R.G. (Eds.), Studies in Maine Geology, Volume 1: Structure and Stratigraphy. Maine Geological Survey, pp. 17–34.

Janssen, C., Michel, W., Bau, M., Luders, V., Muhle, K., 1997. The North Anatolian Fault Zone and the role of fluids in seismogenic deformation. Journal of Geology 105, 387–403.

Kelly, P.J., Sanderson, D.J., Peacock, D.C.P., 1998. Linkage and evolution of conjugate strike-slip fault zones in limestones of Somerset and Northumbria. Journal of Structural Geology 20, 1477–1493.

Knipe, R.J., 1989. Deformation mechanisms—recognition from natural tectonites. Journal of Structural Geology 11, 127–146.

Lin, P., Logan, J.M., 1991. The interaction of two closely spaced cracks: a rock model study. Journal of Geophysical Research 96, 21667–21675.

Logan, J.M., Friedman, M., Higgs, N., Dengo, C., Shimamoto, T., 1979. Experimental studies of simulated gouge and their application to studies of natural fault zones. U.S. Geological Survey Open-File Report 79-1239, pp. 305–343.

Mansfield, C., Cartwright, J., 2001. Fault growth by linkage: observations and implications from analogue models. Journal of Structural Geology 23, 745–763.

Martel, S.J., Pollard, D.D., 1989. Mechanics of slip and fracture along small faults and simple strike-slip fault zones in granitic rock. Journal of Geophysical Research 94, 9417–9428.

Matthai, S.K., Fisher, G., 1996. Quantitative modeling of fault-fluid-discharge and fault-dilation-induced fluid-pressure variations in the seismogenic zone. Geology 24, 183–186.

McGarr, A., Pollard, D., Gay, N.C., Ortlepp, W.D., 1979. Observations and analysis of structures in exhumed mine-induced faults. U.S. Geological Survey Open-File Report 79-1239, pp. 101–120.

Mollema, P.N., Antonellini, M., 1999. Development of strike-slip faults in the dolomites of the Sella Group, Northern Italy. Journal of Structural Geology 21, 273–292.

Morgenstern, N.R., Tchalenko, J.S., 1967. Microscopic structures in kaolin subjected to direct shear. Geotechnique 17, 309–328.

Muraoka, H., Kamata, H., 1983. Displacement distribution along minor fault traces. Journal of Structural Geology 5, 483–495.

Naylor, M.A., Mandl, G., Sijpesteijn, C.H., 1986. Fault geometries in basement-induced wrench faulting under different initial stress states. Journal of Structural Geology 8, 737–752.

Nguyen, P.T., Cox, S.F., Harris, L.B., Powell, C.M., 1998. Fault-valve behavior in optimally oriented shear zones: an example at the Revenge Gold mine, Kambalda, western Australia. Journal of Structural Geology 20, 1625–1640.

Osberg, P.H., Hussey, A.M., Boone, G.M., 1985. Bedrock geologic map of Maine. Augusta, Maine, Maine Geological Survey, scale 1:500,000.

Pachell, M.A., Evans, J.P., 2002. Growth, linkage and termination processes of a 10-km-long strike-slip fault in jointed granite: the Gemini Fault zone Sierra Nevada, California. Journal of Structural Geology 24, 1903–1924.

Peacock, D.C.P., 1991. Displacements and segment linkage in strike-slip fault zones. Journal of Structural Geology 13, 1025–1035.

Poulsen, K.H., Robert, F., 1989. Shear zones and gold: practical examples from the southern Canadian Shield. In: Bursnall, J.T. (Ed.), Mineralization in Shear Zones. Geological Association of Canada Short Course Notes 6, pp. 239–266.

Rabinowicz, E., 1965. Friction and Wear in Materials. John Wiley, New York.

Renard, F., Gratier, J.-P., Jamtveit, B., 2000. Kinetics of crack-sealing, intergranular pressure solution, and compaction around active faults. Journal of Structural Geology 22, 1395–1407.

Riedel, W., 1929. Zur Mechanik Geologischer Brucherscheinungen. Zentralblatt fur Mineralogie, Geologie und Paleontologie 1929B, 354–368.

Robert, F., Boullier, A., Firdaous, K., 1995. Gold-quartz veins in metamorphic terranes and their bearing on the role of fluids in faulting. Journal of Geophysical Research 100, 12861–12879.

Scholz, C.H., 1988. The brittle–plastic transition and the depth of seismic faulting. Geologica Rundschau 77, 319–328.

Scholz, C.H., 1990. The Mechanics of Earthquakes and Faulting. Cambridge University Press, Cambridge. 439pp.

Segall, P., Pollard, D.D., 1980. Mechanics of discontinuous faults. Journal of Geophysical Research 85, 4337–4350.

Segall, P., Rice, J.R., 1995. Dilatancy, compaction, and slip instability of a fluid-infiltrated fault. Journal of Geophysical Research 100, 22155–22171.

Sibson, R.H., 1985. Stopping of earthquake ruptures at dilational fault jogs. Nature 316, 248–251.

Sibson, R.H., 1989. Earthquake faulting as a structural process. Journal of Structural Geology 11, 1–14.

Sibson, R.H., 1990. Faulting and fluid flow. In: Nesbitt, B.E. (Ed.), Fluids in Tectonically Active Regimes of the Continental Crust. Mineralogical Association of Canada, Short Course on Crustal Fluids, Handbook 18, pp. 93–132.

Sibson, R.H., Moore, J.M., Rankin, A.H., 1975. Seismic pumping—a hydrothermal fluid transport mechanism. Journal of the Geological Society of London 131, 653–659.

Sleep, N.H., Blanpied, M.L., 1994. Ductile creep and compaction: a mechanism for transiently increasing fluid pressure in most sealed faults zones. Pure and Applied Geophysics 143, 9–40.

Swanson, M.T., 1988. Pseudotachylyte-bearing strike-slip duplex structures in the Fort Foster Brittle Zone, S. Maine. Journal of Structural Geology 10, 813–828.

Swanson, M.T., 1989. Sidewall ripouts in strike-slip faults. Journal of Structural Geology 11, 933–948.

Swanson, M.T., 1990. Extensional duplexing in the York Cliffs strike-slip fault system, southern coastal Maine. Journal of Structural Geology 12, 499–512.

Swanson, M.T., 1992. Late Acadian–Alleghenian transpressional deformation: evidence from asymmetric boudinage in the Casco Bay area, coastal Maine. Journal of Structural Geology 14, 323–342.

Swanson, M.T., 1999a. Kinematic indicators for dextral shearing along the Casco Bay section of the Norumbega fault zone, coastal Maine. In: Ludman, A., West, D.P. (Eds.), Norumbega Fault System of the Northern Appalachians Boulder Colorado. Geological Society of America Special Paper 331, pp. 1–24.

Swanson, M.T., 1999b. Dextral transpression at the Casco Bay restraining bend, Norumbega fault zone, coastal Maine. In: Ludman, A., West, D.P. (Eds.), Norumbega Fault System of the Northern Appalachians Boulder Colorado. Geological Society of America Special Paper 331, pp. 85–104.

Swanson, M.T., 2005. Geometry and kinematic of adhesive wear in brittle strike-slip fault zones. Journal of Structural Geology 27, 871–887.

Sylvester, A.J., 1988. Strike-slip faults. Geological Society of America Bulletin 100, 1666–1703.

Tchalenko, J.S., 1970. Similarities between shear zones of different magnitude. Geological Society of America Bulletin 81, 1625–1640.

Tchalenko, J.S., Ambraseys, N.N., 1970. Structural analysis of the Dasht-e Bayaz (Iran) earthquake fractures. Geological Society of America Bulletin 81, 41–60.

Vermilye, J.M., Scholz, C.H., 1999. Fault propagation and segmentation: insight from the microstructural examination of a small fault. Journal of Structural Geology 21, 1623–1636.

West, D.P., 1988. $^{40}Ar/^{39}Ar$ mineral ages from southwestern Maine: evidence for Late Paleozoic metamorphism and Mesozoic faulting. M.S. Thesis, University of Maine, Orono, Maine.

West, D.P., Lux, D.R., Hussey, A.M., 1989. $^{40}Ar/^{39}Ar$ mineral ages from the Casco Bay group, southwestern Maine. Geological Society of Americas Abstracts with Programs 20, 78.

Wilcox, R.E., Harding, T.P., Seeley, D.R., 1973. Basic wrench tectonics. American Association of Petroleum Geologists Bulletin 57, 74–96.

Willemse, E.J.M., Peacock, D.C.P., Aydin, A., 1997. Nucleation and growth of strike-slip faults in limestones from Somerset, U.K. Journal of Structural Geology 19, 1461–1477.

Woodcock, N.H., Fischer, M., 1986. Strike-slip duplexes. Journal of Structural Geology 8, 725–735.